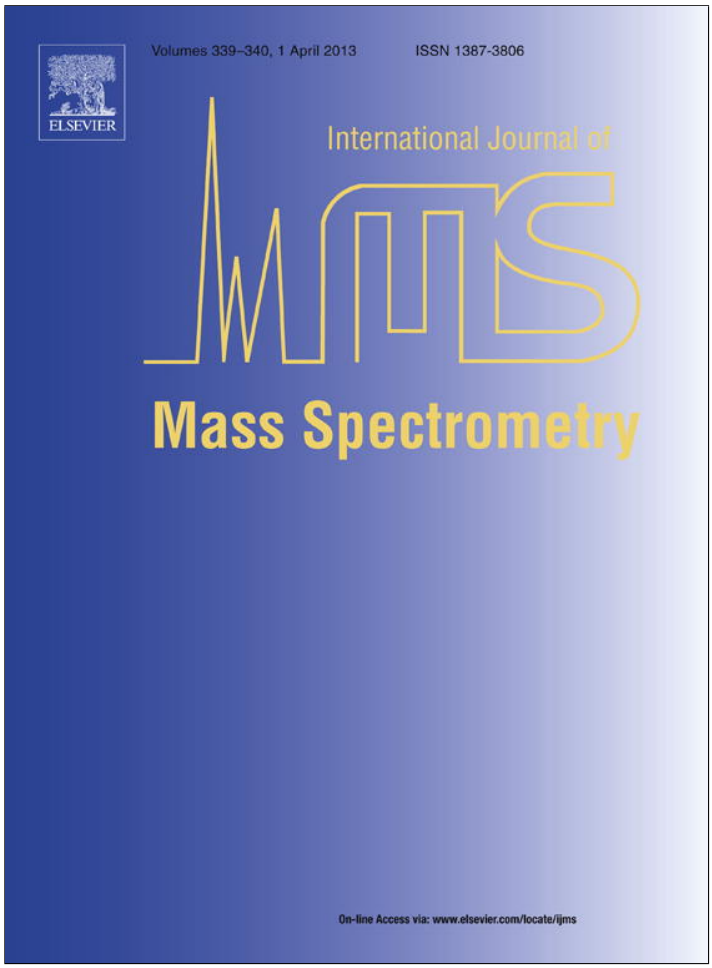

International Journal of Mass Spectrometry 339–340 (2013) 16–23

Contents lists available at SciVerse ScienceDirect

International Journal of Mass Spectrometry

journal homepage: www.elsevier.com/locate/ijms

Electron impact total ionization cross sections for all the components of DNA and RNA molecule

Minaxi Vinodkumar[a,*], Chetan Limbachiya[b], Mayuri Barot[a], Mohit Swadia[b], Avani Barot[a]

[a] V P & R P T P Science College, Vallabh Vidyanagar 388 120, Gujarat, India
[b] P. S. Science College, Kadi 382 715, Gujarat, India

ARTICLE INFO

Article history:
Received 1 November 2012
Received in revised form 9 January 2013
Accepted 9 January 2013
Available online 20 February 2013

PACS:
34
80
Bm

Keywords:
Deoxyribonucleic acid (DNA)
Ribonucleic acid (RNA)
Total ionization cross section
Spherical complex optical potential (SCOP)
Complex scattering potential-ionization contribution (CSP-ic)

ABSTRACT

Present paper reports electron impact total ionization cross sections (Q_{ion}) for all the components of DNA and RNA molecules from threshold to 2000 eV. We have employed spherical complex optical potential (SCOP) formalism to calculate the total inelastic cross sections and have deduced total ionization cross sections using complex scattering potential-ionization contribution (CSP-ic) method. DNA and RNA being the complex molecules, these cross sections are evaluated using the group additivity rule. The present results find good accord with the available previous theoretical estimates. In absence of experimental data for these biomolecules, the present theoretical estimates prove to be the reference data source. Q_{ion} for sugar phosphate backbone of RNA and for complete DNA and RNA units are reported for the first time in this work.

1. Introduction

Electron induced reactions are the most fundamental processes as they drive nearly all the important chemical processes in various sectors of applied physics such as radiation chemistry, plasma etching in semiconductors, stability of waste repositories, the dynamics of the atmosphere and interstellar clouds, dissociative recombination and electron attachment processes. In recent times, the importance of low energy electron impact studies on biomolecules has geared prominence due to the pioneering work of Sanche and coworkers [1,2]. Biomolecules, in particular DNA/RNA components are very sensitive to high energy radiation damage which can occur due to primary, secondary or reactive processes [3]. In irradiated cells, the single and multiple ionization produces large number of secondary electrons that carry large fraction of the energy of the impinging radiation. These low energy electrons (9–20 eV) [4] can interact resonantly or directly with the irradiated biomolecules through series of sequential reactions causing damage to the DNA and the RNA in terms of either single or double strand breaks. The direct interaction can break the backbone of the DNA while the resonances or transient anion formation will dissociate it into neutral and anionic fragments [5]. Thus, to arrive at a complete description of the biological effects of radiation, the entire sequence of events leading to the final chemical state of the cell must be known and the mechanisms involved must be understood. This sequence of events occurs on a timescale ranging from atto seconds to macroscopic times. The complete set of cross sections resulting from low to intermediate energy electron collisions with DNA molecules or its building blocks are needed as input in Monte Carlo analysis which are used to study damage to living cells induced by ionizing radiations [6,7].

The study of total ionization cross sections play an important role in investigating the lesion causing effects of electrons on DNA/RNA molecular components. Despite the importance of electron impact ionization studies with DNA based molecules the data is limited particularly on the experimental front. This is attributed to the fact that the electron scattering experiments with complex biomolecules in the gas phase are challenging because of the difficulties in the preparation of well-characterized pure gas targets of these molecules and the subsequent quantitative determination of the target densities [7]. Hence there is no experimental electron impact ionization data reported for any of the DNA components (adenine, guanine, thymine, cytosine and sugar phosphate backbone) except uracil to the best of our knowledge.

* Corresponding author. Tel.: +91 9723309739; fax: +91 2692 235207.
E-mail address: minaxivinod@yahoo.co.in (M. Vinodkumar).

1387-3806/$ – see front matter © 2013 Elsevier B.V. All rights reserved.
http://dx.doi.org/10.1016/j.ijms.2013.01.004

Table 1
Target properties.

Molecule	Ionization threshold (eV)	Bond lengths (Å)			
Adenine	8.84	C—C	1.14	N—H	1.07
		C—N	1.34	C—H	1.04
Guanine	8.48	C—C	1.49	C—H	1.09
		C—N	1.37	C—O	1.27
Cytosine	9.01	N—H	1.07	C—C	1.39
Thymine	9.48	C—H	1.04	C—O	1.27
Uracil	9.25	C—H	1.09	N—C	1.47
DNA Sugar Backbone	11.74	C—N	1.47	C—C	1.54
RNA Sugar Backbone	11.74	C—H	1.14	O—H	1.04
Phosphate	11.72	P—O	1.59	O—H	1.04

However theoretical ionization cross sections for DNA components are reported by a few groups [8–11]. Electron impact ionization cross sections for adenine, cytosine, guanine, thymine and sugar-phosphate backbone are calculated using the Deutsch–Mark(DM) and the Binary–Encounter–Bethe (BEB) formalisms for energy range between ionization threshold and 1 keV by Bernhardt and Paretzke [11]. Huo et al. [12] reported total ionization cross section for adenine, guanine, thymine, cytosine and uracil using BEB formalism from threshold of the target to 10 keV. Peudon et al. [13] reported total ionization cross sections for adenine, guanine, thymine, cytosine, uracil and sugar phosphate using BEB formalism from threshold of the target to 10 keV. Very recently Vinodkumar and Limbachiya [14] reported electron impact total cross section and total ionization cross sections for uracil and phosphate group from ionization threshold to 2 keV as against a lone measurement reported for total ionization cross section by Feil et al. [6]. They reported electron impact partial ionization cross sections for the formation of three important fragments, $C_4H_4N_2O^{+2}$, $C_3H_3NO^+$ and OCN^+. Feil et al. [6] also reported normalized total single ionization cross section for uracil and calculated total ionization cross section based on the semi-classical DM formalism at 100 eV.

In present work, we report the total ionization cross sections for all components of the DNA and RNA molecules viz. adenine, guanine, thymine, cytosine, uracil and backbone units (sugar phosphate) from threshold of the target to 2 keV. For computing total inelastic cross sections, we employed well established spherical complex optical potential (SCOP) [15,16] formalism and extracted total ionization cross sections using the complex scattering potential-ionization contribution method [17–20]. While other groups [8,9,11,13] have reported the total ionization cross sections using the independent atom model (IAM), we have employed group additivity rule for our calculations. Fig. 1 shows the complete geometrical structure of various components of DNA/RNA molecule along with the bonding structure. It is shown that while DNA structure consists of thymine, adenine, guanine and cytosine as nitrogen base and dioxyribose and phosphate as sugar phosphate backbone molecules, in RNA thymine is replaced by uracil and dioxyribose is replaced by Ribose molecules.

Table 1 lists various target properties of the components of DNA and RNA used for the computation of total ionization cross sections. The detailed theoretical methodology is discussed in the next section.

2. Theoretical methodology

The electron atom/molecule scattering phenomenon is characterized quantitatively by two important cross sections viz. total elastic and total inelastic cross sections and they combine to represent total cross sections. Accordingly we have,

$$Q_T(E_i) = Q_{el}(E_i) + Q_{inel}(E_i) \tag{1}$$

where the first term on the right hand side accounts for all elastic processes while the second term takes care of loss of flux in outgoing channels resulting from electronic excitations and ionization. In the present work we focus the inelastic channel only. The complete spherical complex optical potential [15,16] is represented by,

$$V_{opt}(E_i, r) = V_R(E_i, r) + iV_I(E_i, r) \tag{2}$$

where the real part of the potential V_R consists of static potential (V_{st}), exchange potential (V_{ex}), and polarization potential (V_p). Owing to the fixed nuclei approximation, the static potential (V_{st}) is calculated at the Hartree–Fock level. The exchange potential (V_{ex}) is responsible for electron exchange between the incoming projectile and the target-electrons. The polarization potential (V_p) combines the short range correlation and the long range polarization effect that arises due to the momentary redistribution of target charge cloud which gives rise to dipole and quadrupole moments. The second term of Eq. (2) is the imaginary part of the potential which is taken care by the absorption potential. It is to be noted here that the SCOP as such does not require any fitting parameters. All the potentials described vide Eq. (2) are charge–density dependent. Hence, representation of target charge density is very crucial. We have employed atomic charge density derived from the Hartree Fock wave functions of Bunge and Barrientos [21]. Here DNA/RNA molecules are very complex and their constituents are also large in size. The single center approach will not be feasible and hence we have employed the group additivity method which is better compared to simple additivity rule, which overestimates particularly at low energies. In group additivity we consider geometrical structure of the molecule. The groups where a lighter hydrogen atom is bonded with heavier atom such as C, N and O, the charge density of lighter hydrogen atom is expanded at the center of heavier atom by employing the Bessel function expansion as in Gradshetyn and Ryzhik [22]. This is a good approximation since hydrogen atoms do not significantly act as scattering centers and the cross sections are dominated by the central atom size. In case of the groups having heavier atoms, the molecular charge density is derived from the atomic charge densities by expanding them at the center of mass of the system. Thus, the single-center molecular charge density is obtained by a linear combination of constituent atomic charge densities, renormalized to account for covalent molecular bonding. The molecular charge density $\rho(r)$ so obtained is renormalized to incorporate the covalent bonding as described in our earlier paper [23]. In the SCOP formalism [15], the spherical part of the complex optical potential is used to solve the Schrödinger equation using partial wave analysis to yield various cross sections [15]. Presently our absorption potential is elastic to both vibrational and rotational excitations of the target.

As discussed earlier the absorption potential takes care of loss of flux into all allowed inelastic channels. For this we have used model potential of Staszewska et al. [24] which is non-empirical, quasifree, Pauli-blocking and dynamic in nature. The full form of model potential is represented by,

$$V_{abs}(r, E_i) = -\rho(r)\sqrt{\frac{T_{loc}}{2}} \times \left(\frac{8\pi}{10k_F^3 E_i}\right) \times \theta(p^2 - k_F^2 - 2\Delta)\cdot(A_1 + A_2 + A_3) \tag{3}$$

The parameters A_1, A_2 and A_3 are defined as,

$$A_1 = 5\frac{k_f^3}{2\Delta};\quad A_2 = \frac{k_f^3\left(5p^2 - 3k_f^2\right)}{\left(p^2 - k_f^2\right)^2};$$

$$A_3 = \frac{2\theta\left(2k_f^2 + 2\Delta - p^2\right)\left(2k_f^2 + 2\Delta - p^2\right)^{5/2}}{\left(p^2 - k_f^2\right)^2} \tag{4}$$

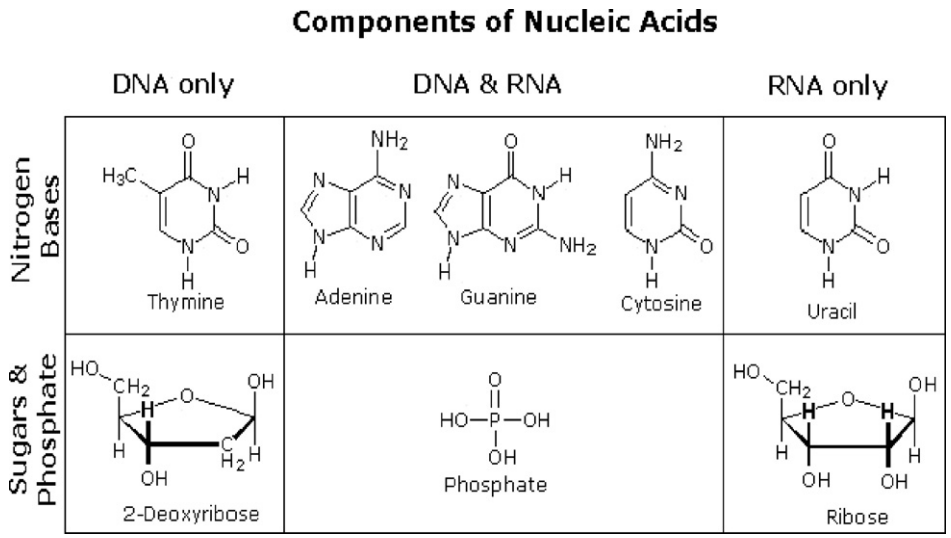

Fig. 1. Geometrical structure of various components of DNA/RNA.

The local kinetic energy of the incident electron is given by,

$$T_{loc} = E_i - (V_{st} + V_{ex}) \tag{5}$$

The dynamic absorption potential is density functional wherein it depends on charge density ($\rho(r)$) of the target, incident energy (E_i) and the parameter Δ of the target. It is sensitive to short range potentials like static and exchange through the term T_{loc} and insensitive to long range potentials like polarization. In Eq. (3), $p^2 = 2E_i$, represents the momentum transfer of incident electron in Hartree, and $k_F = [3\pi^2\rho(r)]^{1/3}$ is the Fermi wave vector. Also, $\theta(x)$ is the Heaviside unit step-function which depends on $\rho(r)$, k_F and Δ, such that $\theta(x) = 1$ for $x \geq 0$, and is zero otherwise. In other words $\theta(x)$ defines the boundary below which the absorption potential is zero and above which it has finite value. The dynamic parameters A_1, A_2 and A_3 of Eq. (3) are the function of $\rho(r)$, I, Δ and E_i. The parameter Δ is very important since it determines a threshold below which $V_{abs} = 0$, implying that the ionization or excitation channels are prevented energetically. This further infers that the Δ parameter represents the threshold energy for continuum states, which means only ionization process is taken into account, excitation to discrete levels being ignored by the original model [25]. So in order to include the excitations due to discrete levels at lower energy, we have considered Δ as the energy dependent parameter. A variable Δ accounts for more penetration of the absorption potential in the target charge-cloud region [17,26–28]. Following the earlier works in this regard [17,26–28], we express Δ as a function of E_i around I as,

$$\Delta(E_i) = 0.8I + \beta(E_i - I) \tag{6}$$

Here, β is obtained by requiring that $\Delta = I$ at $E_i = E_p$, where E_p is the value of E_i at which Q_{inel} attains maximum value. For $E_i > E_p$, Δ is held constant equal to the ionization energy of the target as suggested in the original model of Staszewska et al. [24].

After generating the full complex optical potential given in Eq. (2) for a given electron molecule system, we solve the Schrödinger equation numerically with Numerov method using partial wave analysis. At low incident electron energies with short range potentials, only few partial waves are significant for convergence, e.g., at ionization threshold of the target around 5–6 partial waves are sufficient but as the incident energy increases large number of partial waves are needed for convergence. Using these partial waves the complex phase shifts are obtained which are key ingredients to find the relevant cross sections. The phase shifts contains all the information regarding the scattering event.

Total inelastic cross section is not a directly measurable quantity and hence also not directly comparable quantity. However, experimentally the total inelastic cross sections can be obtained as the difference between experimental values of grand total cross sections (beam attenuation experiments) and purely elastic cross sections (obtained by integrating differential elastic cross sections). In practice few experimental groups are doing both the measurements simultaneously, and different groups work in different energy regimes and their experimental uncertainties are also different and hence there is difficulty in obtaining total inelastic cross sections from the experiment. But, it is one of the most important quantities as it contains the ionization and electronic excitations which are directly measurable quantities. Thus, we partition the total inelastic cross sections into its two vital components; one due to the discrete electronic excitations and other due to the continuum ionization contribution, as,

$$Q_{\text{inel}}(E_i) = \sum Q_{exc}(E_i) + Q_{ion}(E_i) \tag{7}$$

Here, first term represents the sum over total excitation cross sections for all accessible electronic discrete transitions, while the second term is the total cross sections due to all allowed electronic transitions to continuum i.e., ionization. In the present range of energies it is the single ionization that dominates in Eq. (7). The discrete transitions arise mainly from the low-lying dipole allowed transitions for which the cross section decreases beyond E_p. By definition,

$$Q_{\text{inel}}(E_i) \geq Q_{ion}(E_i) \tag{8}$$

This is an important inequality and it forms the basis for CSP-ic method. Total ionization cross section may be estimated from total inelastic cross section by defining an energy dependent ratio $R(E_i)$ given by,

$$R(E_i) = \frac{Q_{ion}(E_i)}{Q_{\text{inel}}(E_i)} \tag{9}$$

such that, $0 < R \lesssim 1$.

As total ionization cross section is a continuous function of energy, we can express this ratio also as a continuous function of energy for $E_i > I$, used in earlier studies as [17,26–28].

$$R(E_i) = 1 - f(U) = 1 \quad - \quad C_1\left(\frac{C_2}{U+a} + \frac{\ln(U)}{U}\right) \tag{10}$$

here, U is the dimensionless variable defined by, $U = E_i/I$.

The reason for adopting such an explicit form of $f(U)$ could be visualized as follows. At high energies the total inelastic cross section follows the Born Bethe term according to which the cross sections falls of as $\ln(U)/U$, but at low and intermediate energies they obey $1/E$ form [29]. Accordingly, the first term will take care of the cross sections behavior at low and intermediate energies while the second term will take care at high energies. The dimensionless parameters C_1, C_2 and 'a' involved in the above equation are deduced by imposing the three conditions on the ratio as discussed below.

$$R(E_i)\begin{cases} = 0 \quad for \quad E_i \le I \\ = R_p \quad for \quad E_i = E_p \\ \cong 1 \quad for \quad E_i \gg E_p \end{cases} \tag{11}$$

The first condition is an exact condition wherein it states that no ionization process is possible below the ionization threshold of the target implying that the value of the ratio must be zero. Coming to the last condition, which physically states that ionization contribution is almost equal to inelastic contribution at very high ($\sim$10 E_p) energies, this is attributed to the fact that at such high energies there are innumerable channels open for the ionization as against very few finite channels for excitation. At such high energies the contribution of excitation is almost negligible. Thus the ratio approaches unity.

The second condition is very crucial and empirical in nature. R_P is the value of R at $E_i = E_p$, and it was observed that at the peak of inelastic cross section the contribution for ionization is about 70–80%. This argument is supported by many targets studied through CSP-ic [30]. This behavior is attributed to the faster fall of the contribution of the first term $\Sigma Q_{ecx}\, Q_{exc}$ in Eq. (10) to the total inelastic cross sections, hence we choose $R_p = 0.7$. Choosing a single value will make our method consistent and predictive. For calculating Q_{ion} from Q_{inel} we need R as a continuous function of energy for $E_i > I$. Hence we represent the ratio R in the following manner.

$$R(E_i) = 1 - f(U) \tag{12}$$

Presently the above ratio has been determined using the following analytical form

$$R(E_i) = 1 - C_1\left(\frac{C_2}{U+a} + \frac{\ln(U)}{U}\right) \tag{13}$$

where U is the dimensionless variable defined by, $U = E_i/I$.

We have adopted this particular functional form for $f(U)$ in Eq. (13) due to its behavior with respect to the incident energy. As E_i increases above I, the ratio R increases and approaches unity, since the ionization contribution rises and the discrete excitation term in Eq. (10) decreases. The discrete excitation cross sections, dominated by dipole transitions, fall off as $ln(U)/U$ at high energies. Accordingly the decrease of the function $f(U)$ must also be proportional to $ln(U)/U$ in the high range of energy. However, the two-term representation of $f(U)$ given in Eq. (13) is more appropriate since the first term in the bracket ensures a better energy dependence at low and intermediate E_i. The dimensionless parameters C_1, C_2, and a, involved in Eq. (13) depends on the properties of the target under investigation. The three conditions stated in Eq. (11) are used to determine these three parameters and hence the ratio R. This is called the CSP-ic method. Evaluating Q_{ion} through CSP-ic method

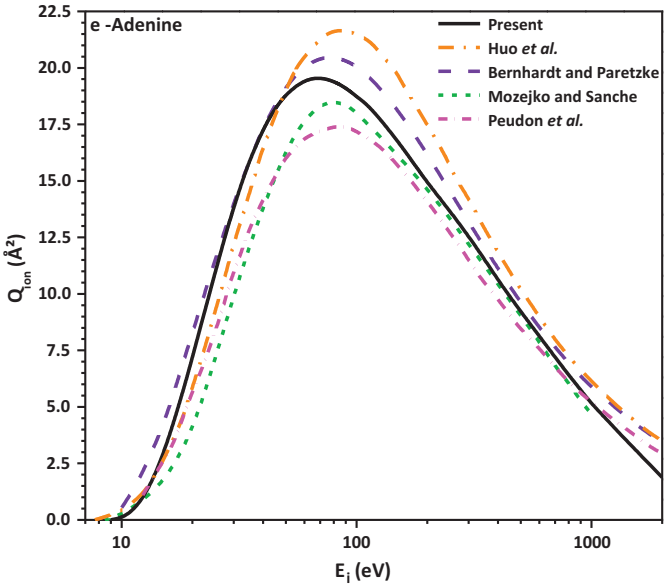

Fig. 2. Total ionization cross section for e-Adenine. Solid line: present results, short dash line: Mozejko and Sanche [8], dash line: Bernhardt and Paretzke [11], dash dot line: Huo et al. [12] and short dash dot line: Peudon et al. [13].

[17,26–29], the summed excitations cross sections, $\sum Q_{exc}$, can be easily calculated vide Eq. (10).

3. Results and discussion

The theoretical approach of SCOP is employed to determine total inelastic cross sections, Q_{inel}, and the CSP-ic method outlined above is employed to calculate the total ionization cross sections, Q_{ion} along with a useful estimation of electronic excitations in terms of the summed total excitation cross sections $\sum Q_{exc}$. The ionization cross sections of Adenine, Guanine, Thymine, Cytosine, uracil and Sugar-phosphate backbones for RNA and DNA molecules are plotted as function of projectile energy from circa threshold of the target to 2 keV vide Figs. 2–8 respectively. Fig. 9 represents the mutual comparison of total ionization cross sections for all the

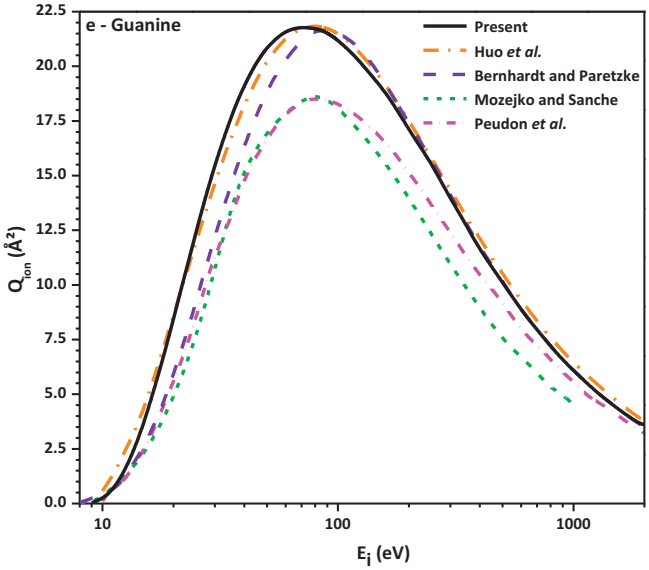

Fig. 3. Total ionization cross section for e-Guanine. Solid line: present results, short dash line: Mozejko and Sanche [8], Dash line: Bernhardt and Paretzke [11], dash dot line: Huo et al. [12] and short dash dot line: Peudon et al. [13].

Table 2
Total ionization cross sections in Å^2.

Energy (eV)	Adenine	Guanine	Thymine	Cytosine	Uracil	DNA backbone	RNA backbone	Phosphate
9	0.004	0.029	0.000	0.000	0.000	0.000	0.000	0.000
10	0.095	0.218	0.002	0.019	0.085	0.000	0.000	0.000
11	0.362	0.621	0.056	0.138	0.987	0.000	0.000	0.000
12	0.811	1.216	0.222	0.390	1.158	0.020	0.022	0.025
15	2.923	3.725	1.422	1.784	2.846	0.797	0.885	0.569
20	7.196	8.443	4.640	4.848	6.913	4.481	4.933	2.174
25	10.944	12.441	7.970	7.574	10.111	9.559	10.440	3.967
30	13.812	15.456	10.820	9.650	12.166	14.568	15.828	5.666
36	16.177	17.952	13.396	11.375	13.446	18.952	20.562	7.717
40	17.246	19.104	14.638	12.167	14.250	21.012	22.797	8.651
46	18.322	20.305	15.969	12.984	14.714	23.210	25.188	9.570
50	18.792	20.847	16.600	13.350	15.029	24.144	26.216	9.903
60	19.421	21.588	17.547	13.843	15.227	25.350	27.575	10.253
70	19.548	21.775	17.868	13.944	15.237	25.654	27.958	10.319
80	19.394	21.730	17.846	13.858	15.223	25.476	27.816	10.293
90	19.103	21.523	17.806	13.749	14.900	25.065	27.414	10.199
100	18.733	21.187	17.599	13.545	14.974	24.548	26.888	10.051
200	14.930	16.612	14.598	11.023	12.526	19.173	21.139	8.168
500	9.218	10.515	9.218	5.998	8.12079	11.329	12.516	5.063
1000	5.111	5.753	5.760	3.287	4.97655	6.960	7.684	3.200
2000	1.879	3.600	3.303	1.004	2.79977	4.009	4.423	1.883

targets studied in this work. Fig. 10 shows the total ionization cross section for the complete DNA and RNA molecule. The numerical values of the total ionization cross sections are tabulated in Table 2 for ready reference.

Fig. 2 shows comparison of present total ionization cross section for e-Adenine scattering with available results. No experimental ionization data are available for comparison to the best of our knowledge. The theoretical results are provided by Huo et al. [12], Bernhardt and Partezke [11], Mozejko and Sanche [8] and Peudon et al. [13]. Huo et al. [12], Mozejko and Sanche [8] and Peudon et al. [13] have employed BEB formalism. It can be clearly visualized from the figure that though same formalism is employed by the above mentioned authors [8,12,13], there are variations in their results as BEB is parameter dependent formalism. The present results are found to be in general agreement with all other data and are in best accord with the results of Bernhardt and Partezke [11], who employed DM formalism. The results of Huo et al. [12] are in very good agreement with present results up to 70 eV, but at the peak they are higher compared to all data presented here and beyond 200 eV again they are in good accord with the present results. The results of Mozejko and Sanche [8] are lower compared to all results presented here up to the peak and beyond it they are in very good agreement with the present results. The results of Peudon et al. [11] are very similar to the results of Mozejko and Sanche [8] but at the peak their values are slightly lower compared to all the results. Surprisingly, both the authors [12,13] have used BEB formalism and still the variation in their results at the peak is ∼20%.

Fig. 3 shows the comparison of present total ionization cross sections for e-Guanine scattering with the available comparisons. While, Huo et al. [12], Mozejko and Sanche [8] and Peudon et al. [13] employed BEB formalism, Bernhardt and Partezke [11] employed DM formalism to compute total ionization cross sections. We observe that while the results of Huo et al. [12] are in very good agreement with present results throughout the energy range, the results of Bernhardt and Paretzke [11] are lower compared to present results up to the peak but beyond it they are in excellent

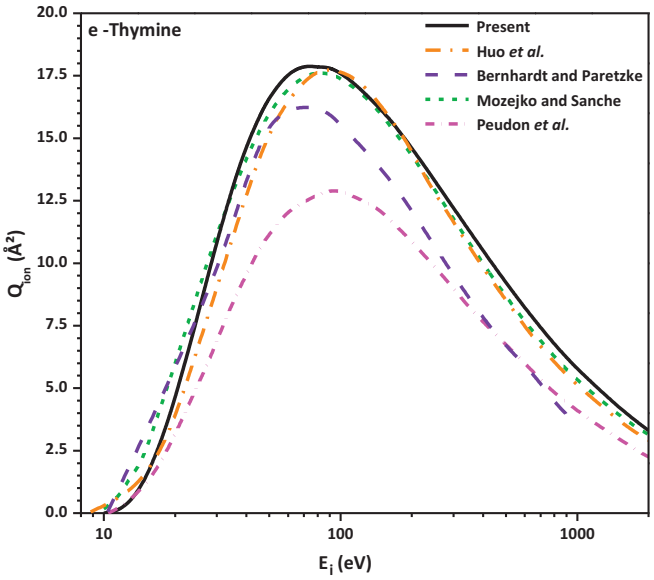

Fig. 4. Total ionization cross section for e-Thymine. Solid line: present results, short dash line: Mozejko and Sanche [8], dash line: Bernhardt and Paretzke [11], dash dot line: Huo et al. [12] and short dash dot line: Peudon et al. [13].

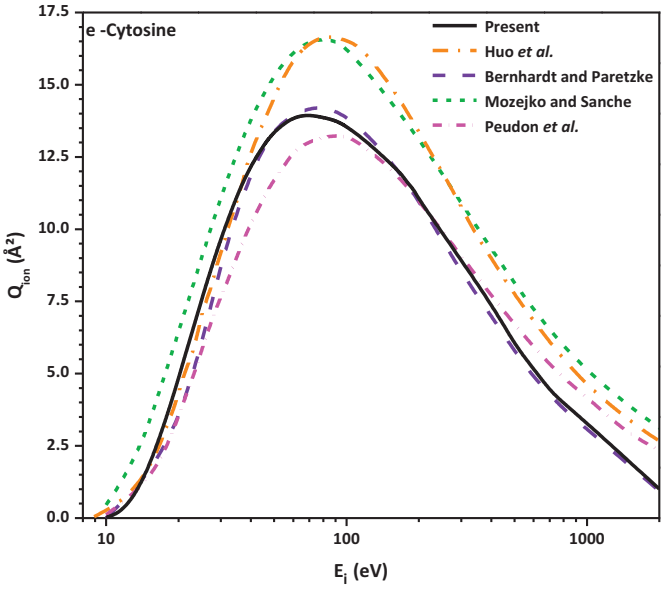

Fig. 5. Total ionization cross section for e-Cytosine. Solid line: Present results, Short Dash line: Mozejko and Sanche [8], Dash line: Bernhardt and Paretzke [11], Dotted line: Huo et al. [12] and Short Dot Dash line: Peudon et al. [13].

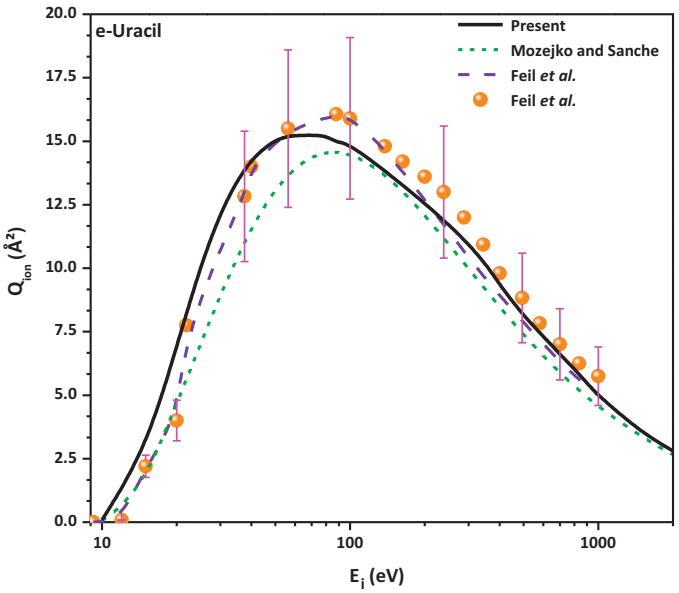

Fig. 6. Total ionization cross section for e-Uracil. Solid line: present results, short dash line: Mozejko and Sanche [8], dash line: Feil et al. [6], open squares: Feil et al. [6].

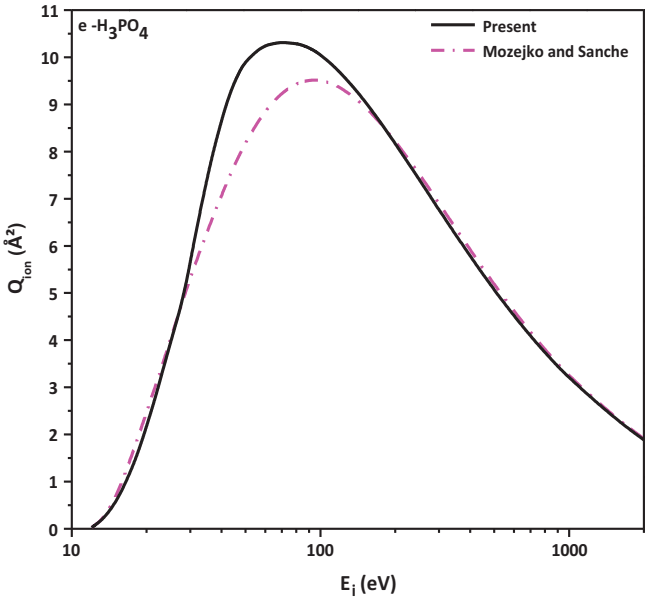

Fig. 8. Total ionization cross section of H_3PO_4. Solid line: present results and dash-dot line: Mozejko and Sanche [8].

agreement with the present results. The results of Mozejko and Sanche [8] and Peudon et al. [13] are similar up to the peak and are lower by 14% at the peak compared to the present results. Beyond the peak, the results of Mozejko and Sanche [8] are the lowest compared to all the results presented here. Again in this case the difference in the results obtained using BEB formalism [12,13] is 14% near the peak.

A comparison of present total ionization cross sections for e-Thymine scattering is shown along with other theoretical estimates in Fig. 4. The BEB data of Mozejko and Sanche [8] and Huo et al. [12] are in excellent agreement with the present data throughout the impact energy range. The BEB results of Peudon et al. [13] are the lowest compared to all the results at the peak and the variations among the BEB results of [8,12,13] are about 28%. The DM results of Bernhardt and Paretzke [11] are in agreement with the present results up to 50 eV beyond which they suddenly drop and are lower compared to the present results.

Fig. 5 shows comparison of present total ionization cross sections for e-Cytosine scattering with the available results. The results of Bernhardt and Paretzke [11] obtained using DM formalism are in very good accord with present results throughout the impact energy range. The results of Peudon et al. [13] are in good agreement with present data throughout the energy range except near the peak where they are lower compared to present results. The results of Huo et al. [12] obtained using BEB formalism are in good agreement with the present results up to 30 eV, above which they are higher compared to present results. The results of Mozejko and Sanche [8] are higher compared to the present

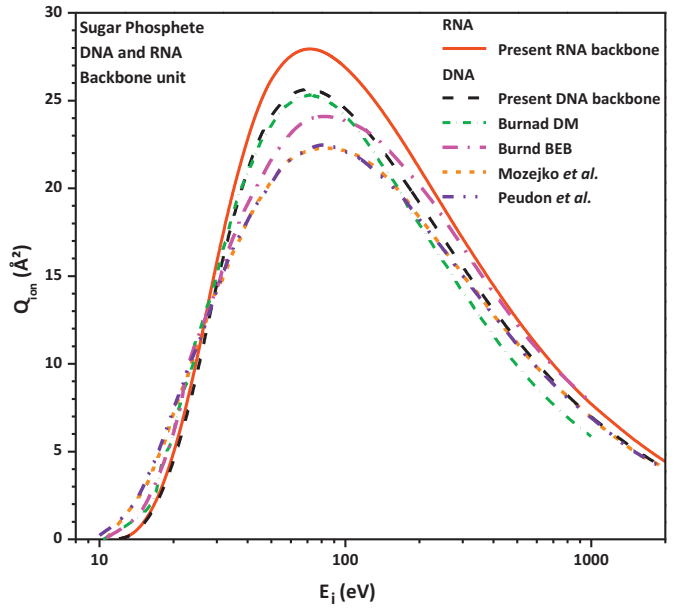

Fig. 7. Total ionization cross sections for DNA and RNA backbone. Solid line: present RNA backbone; dash line: present DNA backbone; short dash-dot line: Burnad (DM); dash-dot line: Burnd BEB; short dash line: Mozejko et al. [9] and dash-dot-dot line: Peudon et al. [13].

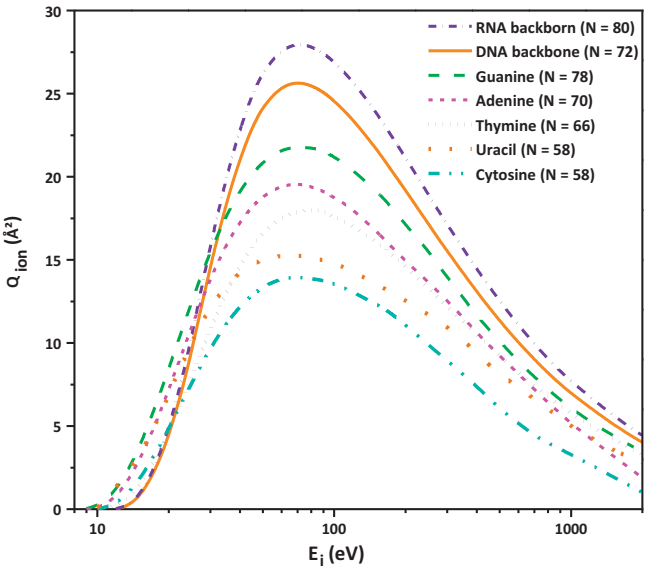

Fig. 9. Total ionization cross sections. Dash-dot: RNA backbone; solid line: DNA backbone; short dash dot line: guanine; short dash line: adenine; dash line: thymine; dotted line: uracil and dash-dot-dot line: cytosine.

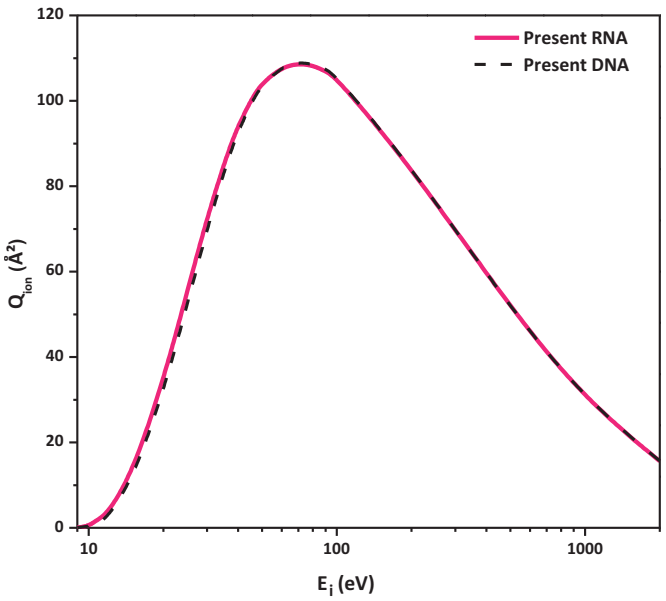

Fig. 10. Total ionization cross sections for DNA (short dash line) and RNA (dash-dot line) molecules.

results throughout the energy range. The results obtained using BEB formalism [8,11,13] differ by 20% near the peak.

In order to report the results of all the components of RNA molecule, we show in Fig. 6 our recent results of total ionization cross section for e-Uracil scattering [14] with available results. This is the only component of RNA molecule for which an experimental work is reported by Feil et al. [6] and our results are in good accord with this measurements and with their theoretical data [6,8] throughout the energy range. However, the present results are lower than the results of Mozejko and Sanche [8] up to 100 eV then after they match well.

Fig. 7 represents the comparison of present total ionization cross sections for sugar phosphate backbone for DNA and RNA molecule. The total ionization cross section for sugar phosphate backbone for DNA molecule is calculated by Bernhardt and Paretzke [11], Mozejko et al. [9] and Peudon et al. [13]. These authors [9,11,13] have used BEB formalism while Bernhardt and Paretzke [11] used both BEB and DM formalism for computation of total ionization cross section. Present data is in excellent agreement with the DM data of Bernhardt and Paretzke [11] throughout the impact energy range. Present data is also in good accord with the BEB data of Mozejko et al. [9], Peudon et al. and Bernhardt and Paretzke [11] for the complete energy range except a slight variation near the peak region. The present peak energy coincides with all the data presented here. The total ionization cross section for sugar phosphate backbone of RNA molecule is presented for the first time. The structural difference between RNA and DNA backbone is that RNA backbone has additional O atom compared to DNA. Hence it is expected that total ionization cross section for RNA backbone should be higher compared to DNA backbone which is reflected in the curve.

The comparison of present total ionization cross sections for e-H_3PO_4 scattering is shown in Fig. 8 along with the lone theoretical results of Mozejko and Sanche [8]. The present results of total ionization cross sections finds excellent agreement with the results of Mozejko and Sanche [8] for complete energy range except between 30 and 100 eV where present results are slightly higher. There is no other theoretical or experimental data for ionization cross sections of phosphoric acid to the best of our knowledge.

Finally in Fig. 9 we present mutual comparison of total ionization cross sections for all the targets studied in this work. The cross sections increase with the increase in geometrical size of the target. This can be roughly estimated from the total number of electrons in the target which are listed in Fig. 9. Among the purines and pyrimidines, guanine has maximum ionization cross sections followed by adenine, thymine, uracil and cytosine. Among the sugar phosphate groups, RNA has highest cross sections compared to the DNA. It is also noted that at high energies the cross sections resulting from all the targets merge revealing the fact that the time spent by the electrons in the vicinity of the target decreases thereby decreasing the cross sections. Also, it is to be noted that the peak energy for the cross sections is very close for all the targets, this is attributed to nearly same ionization thresholds (see Table 1) for all the targets. Such a mutual study of ionization cross sections is important as it enable us to trace the sequential biochemical steps in the mechanism of radiation damage and to develop a more rigorous biochemical model [12].

In Fig. 10 we have shown the total ionization cross sections for the composite DNA and RNA structure. The composite DNA structure includes adenine, guanine, cytosine, thymine, phosphoric acid and sugar phosphate backbone. The composite RNA structure includes adenine, guanine, cytosine, uracil, phosphoric acid and sugar phosphate backbone. No comparison either theoretical or experimental is available to the best of our knowledge. It is seen that when electron interactions are considered with the DNA or RNA the position of their peak and the magnitude of ionization are nearly same. By this we infer that as far as electron driven processes such as lesions caused by secondary electrons generated through irradiation are concerned, both DNA and RNA structures will be affected identically.

4. Conclusion

Present paper reports comprehensive study of electron impact total ionization cross sections for all the components of DNA and RNA molecules along with sugar phosphate backbone unit. It is quite evident from the plots (Figs. 2–8) given in the previous section that present theory accounts for the ionization channel very well. The overall shape and strength of ionization cross section is nicely matched with the previous data for all the targets studied here. In Figs. 9 and 10 we have reported the mutual comparison of total ionization cross sections for all the components of DNA and RNA molecules and the cross sections for composite DNA/RNA systems respectively. The study reflects three facts; the ionization cross section increases with increase in geometric size of the target, the peak of ionization cross section is largely governed by the ionization threshold of the target and for electron driven effects, the DNA and RNA systems are identically affected. Present study has given us the confidence in our calculation and hence we are convinced that present method can reproduce reliable cross section data for complex targets with adequate accuracy and speed. It is thus believed that such efforts will be more appreciated by the technology where cross section data is necessary for further modeling of their systems. Also, we hope that our effort will encourage experimentalists to perform measurements of these important targets.

Acknowledgements

Minaxi Vinodkumar acknowledges DST, New Delhi, for the major research project (SR/S2/LOP/26-2008) and Chetan Limbachiya thanks UGC, New Delhi, for the major research project [F. No. 40-429/2011 (SR)] for financial support under which part of this work is carried out.

References

[1] B. Boudai, P. Cloutier, D. Hunting, M.A. Huels, L. Sanche, Science 287 (2000) 1658.

[2] L. Sanche, Mass Spectrometry Reviews 21 (2002) 349.
[3] L. Sanche, in: M. Greenberg (Ed.), Radical and Radical Ion Reactivity in Nucleic Acid Chemistry, John Wiley & Sons, Inc., 2009, pp. 239–293.
[4] S.M. Pimblott, J.A. LaVerne, Radiation Physics and Chemistry 76 (8–9) (2007) 1244.
[5] M.A. Huels, B. Boudaiffa, P. Cloutier, D. Hunting, L. Sanche, Journal of the American Chemical Society 125 (2003) 4467.
[6] S. Feil, K. Gluch, S. Matt-Leubner, P. Scheier, J. Limtrakul, M. Probst, H. Deutsch, K. Becker, A. Stamatovic, T.D. Mark, Journal of Physics B: Atomic Molecular and Optical Physics. 37 (2004) 3013.
[7] R.H. Ritchie, R.N. Hamm, J.E. Turner, H.A. Wright, W.E. Bloch, Physical and Chemical Mechanisms in Molecular Radiation Biology, Plenum Press, New York, 1991, 99.
[8] P. Mozejko, L. Sanche, Radiation Physics and Chemistry 73 (2005) 77.
[9] P. Mozejko, A. Domaracka, E. Ptasinska-Denga, C. Szmytkowski, Chemical Physics Letters 429 (2006) 378.
[10] A. Dora, L. Bryjko, T. Mourik, J. Tennyson, Journal of Chemical Physics 136 (2012) 024324.
[11] Ph. Bernhardt, H.G. Paretzke, International Journal of Mass Spectrometry 223/224 (2003) 599.
[12] W.M. Huo, C.E. Dateo, G.D, Fletcher, NASA Technical Report, NAS-06-009 (2006).
[13] A. Peudon, S. Edel, M. Terrissol, Radiation Protection Dosimetry http://dx.doi.org/10.1093/rpd/ncl452 (2006).
[14] M. Vinodkumar, C. Limbachiya, Molecular Physics 111 (2013) 213.
[15] A. Jain, Physical Review A 34 (1986) 3707.
[16] A. Jain, K.L. Baluja, Physical Review A 45 (1992) 202.
[17] M. Vinodkumar, K. Korot, H. Bhutadia, International Journal of Mass Spectrometry 294 (2010) 54.
[18] K.N. Joshipura, M. Vinodkumar, C.G. Limbachiya, B. Antony, Physical Review A 69 (2004) 022705.
[19] M. Vinodkumar, K.N. Joshipura, C. Limbachiya, N.J. Mason, Physical Review A 76 (2006) 022721.
[20] M. Vinodkumar, C.G. Limbachiya, K. Korot, K.N. Joshipura, European Physical Journal D 48 (2008) 333.
[21] C.F. Bunge, J.A. Barrientos, Atomic Data and Nuclear Data Tables 53 (1993) 113.
[22] I. Gradashteyn, I.M. Ryzhik, Tables of Integrals, Series and Products, Associated Press, New York, 1980.
[23] M. Vinodkumar, K.N. Joshipura, N.J. Mason, Acta Physica Slovaca 56 (2006) 521.
[24] G. Staszewska, D.W. Schwenke, D. Thirumalai, D.G. Truhlar, Physical Review A 28 (1983) 2740.
[25] F. Blanco, G. Garcia, Physical Review A 67 (2003) 022701.
[26] M. Vinodkumar, R. Dave, H. Bhutadia, B.K. Antony, International Journal of Mass Spectrometry 292 (2010) 7.
[27] M. Vinodkumar, K.N. Joshipura, C.G. Limbachiya, B.K. Antony, Atomic Structure and Collision Processes, Narosa Publishing House, 2009, 177.
[28] M. Vinodkumar, C. Limbachiya, H. Bhutadia, Journal of Physics B: Atomic Molecular and Optical Physics 43 (2010) 015203.
[29] K.N. Joshipura, B.K. Antony, M. Vinodkumar, Journal of Physics B: Atomic Molecular and Optical Physics 35 (2002) 4211.
[30] M. Vinodkumar, K. Korot, P.C. Vinodkumar, International Journal of Mass Spectrometry 305 (2011) 26.